Article

Predictive Modelling of Sea Debris around Maltese Coastal Waters

Mark Dingli [1,*], **Kristian Guillaumier** [2] **and Adam Gauci** [3]

1 Science in Information Technology (Artificial Intelligence), University of Malta, 2080 Msida, Malta
2 Department of Artificial Intelligence, Faculty of Information & Communication Technology, University of Malta, 2080 Msida, Malta; kristian.guillaumier@um.edu.mt
3 Department of Geosciences, Faculty of Science, University of Malta, 2080 Msida, Malta; adam.gauci@um.edu.mt
* Correspondence: mark.dingli.21@um.edu.mt

Abstract: The accumulation of sea-surface debris around the coastal waters of Malta poses significant ecological and environmental challenges, negatively affecting marine ecosystems and human activities. This issue is exacerbated due to the lack of an effective system tailored to predict surface-debris movement specifically for the Islands of Malta. To address this gap, a pipeline that combines a machine learning-based prediction system with a physics-based model is proposed. This pipeline uses data on historical sea-surface current velocities to forecast future conditions and visualise debris movement. Central to this system are two machine learning models trained to predict surface velocities for the next 24 h for a specific area. These predictions are then utilised in a Lagrangian model to simulate and visualise the debris movement, providing insights into future dispersion patterns. A comparative evaluation of both models using real-world data is made to determine which one performs best in this application. This method offers a tailored approach to addressing sea-surface debris around Malta by accurately predicting sea-surface current velocities and visualising debris movement, improving cleanup operations and marine conservation strategies.

Keywords: machine learning; geosciences; Lagrangian simulation; prediction of sea-surface current velocities; oceanography; environmental modelling; marine debris simulation; marine conservation

1. Introduction

Sea-surface debris around the coastal waters of Malta presents a significant environmental issue. Predominantly composed of plastics, which constitute 82% of all man-made floating materials encountered in the Mediterranean Sea [1], this debris endangers marine life, disrupts ecological balance, and compromises the ecological integrity of coastal areas [2]. Studies reveal significant negative effects, ranging from harm to marine wildlife due to ingestion and entanglement [3] to the disruption of natural habitats [4]. The impact on coastal ecosystems extends beyond the environment, affecting economic sectors reliant on marine health, such as tourism and fishing [4]. Further research covers the long-term ecological consequences, highlighting the urgent need for effective management and mitigation strategies, as discussed in [5]. This problem is further aggravated by the lack of an effective system that can predict the movement of this surface debris since, as of this writing, there exists no system that addresses this challenge for the coastal areas around Malta.

Recent advances in predictive modelling for marine debris movement have integrated various techniques to enhance the accuracy and applicability of forecasts. Studies such as those by E. van Sebille et al. [6] have underscored the effectiveness of numerical simulations in capturing the complex dynamics of marine debris dispersal, utilising comprehensive data sets to model environmental interactions [7]. Additionally, the incorporation of deep learning algorithms, as explored by W. R. Winans et al. [8], has proven instrumental in

analysing extensive data sets to detect and categorise debris, which enhances the capabilities of responding to marine pollution. Furthermore, advanced simulation tools like the OceanParcels toolkit [9] have been pivotal in tracing debris pathways, with researchers like M. Yuniarti et al. [10] demonstrating their utility in mapping microplastic distribution. These methodologies collectively offer a detailed understanding of debris behaviour, establishing a robust framework for developing predictive models that are essential for environmental management and conservation.

In this research, a machine learning (ML) technique and a physics-based Lagrangian model [11] are proposed to address environmental issues of sea-surface debris. At the core of this study is a pipeline that uses historical data to predict the next 24 h of sea-surface current (SSC) velocities. These predictions serve as inputs to a Lagrangian model, enabling it to simulate the movement of surface marine debris. In this study, long short-term memory (LSTM) and gated recurrent unit (GRU) models are used due to their ability to deal with the kind of time series data being considered [12]. Both models are then evaluated and compared with a focus on their predictive accuracy and the quality of their visualisations. This offers valuable insights into marine conservation efforts and enhances decision-making processes for the management of marine debris around the Maltese Islands.

1.1. Motivation

The geological characteristics of the Mediterranean Sea make it difficult for surface debris to escape the area naturally, resulting in it accumulating [13]. The current absence of a predictive system tailored to the coastal regions of Malta impedes effective interventions to mitigate environmental harm. This gap opens an opportunity for the implementation of a system that aims to address an urgent ecological issue, which is widely recognised as a global crisis [14]. By fulfilling this need, this research aims to provide accurate predictions that can guide effective cleanup operations and inform strategies for long-term marine conservation around the coast of Malta.

1.2. Aims and Objectives

This study aimed to create a system that simulates and predicts the movement of marine debris in the coastal waters of Malta, thereby supporting marine conservation efforts. To achieve this, several objectives were identified. The sea-surface current (SSC) velocity data sets obtained from the HF Radar Network, operated and maintained by the Department of Geosciences at the University of Malta, was preprocessed and organised to ensure compatibility and consistency for input into the ML and Lagrangian models. The ML models were necessary to predict future SSC velocities, and the Lagrangian physics model was used to accurately simulate debris movement and dispersal. Following extensive experimentation, it was found that LSTM and GRU models hold the most promise in terms of accuracy and real-time performance. Both models were evaluated to determine which one is able to predict sea-surface currents better. Beyond an assessment of the accuracy of both models, a detailed geospatial analysis was performed to better understand the conditions which make one model perform better than the other. The source code and data sets used in this study are publicly accessible on GitHub (https://github.com/markdingli18/FYP_Mark_Dingli, accessed on 29 August 2024).

2. Materials and Methods

The approach taken in this study started out with the management and preprocessing of the SSC data set to ensure data integrity and accuracy. Following this, ML models were implemented that were capable of predicting SSC velocities with high precision. The final phase of the methodology involved developing a physics-based Lagrangian model that integrated the predicted SSC data. This model was used to simulate and visualise the movement and dispersion patterns of sea-surface debris around the Maltese Islands.

2.1. The SSC Data Set

In this study, a data set provided by the Department of Geosciences at the University of Malta was used (https://www.um.edu.mt/science/geosciences, accessed on 29 August 2024). This data set consists of data on SSC velocities recorded in hourly increments across four years, spanning from January 2020 to December 2023. These data points were derived from high-frequency (HF) radar systems [15], located in the northern regions of the Maltese Islands and southern Sicily. The locations of these radar systems, depicted in Figure 1, provide a temporal snapshot of the SSC movements.
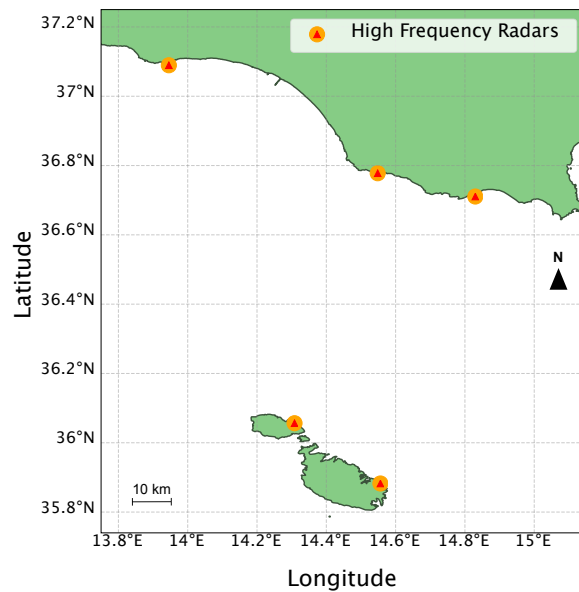
Figure 1. High-frequency radar locations highlighted in orange.

The data are composed of several variables, including longitude, latitude, time, and SSC velocities denoted as west–east velocity (*u*) and north–south velocity (*v*). The data's geographical scope was defined within the boundaries of 14.15° E to 14.81° E in longitude and 35.79° N to 36.30° N in latitude. This coverage translated into a grid totalling 180 data points, as shown in Figure 2. The data set is in the Network Common Data Form (NetCDF) format [16], a commonly used format for climate and meteorological data, ensuring compatibility with the Lagrangian model.
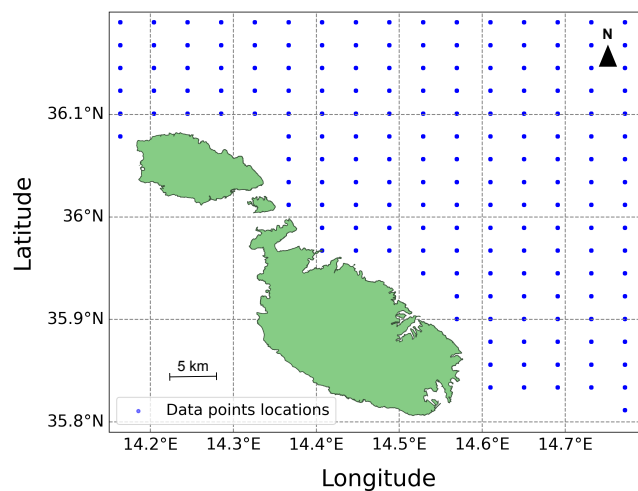
Figure 2. Locations of radar data points.

2.2. The Lagrangian Model

The practice of tracking ocean surface movements in a Lagrangian framework dates back to the earliest days of oceanography. Early methods involved observing the drift of ships or the paths of specially designed floats to document sea-current movements, as outlined by [17]. The Lagrangian model [11] plays a pivotal role in environmental simulations. By offering a dynamic method to trace individual particle trajectories within fluid mediums, the model ensures the precise tracking of the particle's spatiotemporal movement. Its broad applicability spans from localised studies to global-scale systems. This is evident in its varied applications, such as tracking oil-spill diffusion [18], mapping floating plastic debris [19], and simulating jellyfish migrations [20], and smoke dispersion [21].

The Lagrangian model operates by representing particles within a fluid medium, tracking their position and properties as they move with the fluid's flow. The model calculates each particle's trajectory by integrating the fluid's velocity field, which may vary in time and space. This approach enables the simulation of the dispersal patterns of particles, such as marine debris, by accounting for both advection and diffusion processes. Advection represents the movement of particles through the flow of a fluid [22]. Diffusion, on the other hand, models the dispersion of particles through random motion [22]. This is done by applying techniques such as random walks or Gaussian distributions. This inclusion of randomness enhances the realism of simulations.

To facilitate these Lagrangian simulations, several Python toolkits like OceanParcels [9], PyGnome [23], and Flexpart [24] have been developed. These toolkits enable the customisation and execution of particle-tracking simulations, leveraging data on ocean currents, wind fields, and other environmental phenomena. OceanParcels is distinguished by several features that make it suitable for this work. One of its notable capabilities is custom kernels. These are user-defined functions that allow for tailored simulation scenarios at each time step. Through custom kernels, users can implement complex behaviours and interactions of particles within a fluid, such as particle reflection or the response to environmental variables like temperature and wind. Another significant feature is particle initialisation. This feature enables the creation of particles at specific locations and times, and with distinct properties, allowing for more detailed and accurate simulations.

2.3. Time-Series Modelling

Time-series modelling is a technique used to predict future data points by analysing the trends, cycles, and patterns in a series of data points collected over an interval of time [25]. The main focus is on analysing historical data to uncover the underlying structure of the data, which can then be used to forecast future trends. This method is particularly powerful due to its ability to incorporate the sequence and time dependence within a data set. By examining how values are interconnected over time, time-series models can forecast future values based on the inherent temporal dynamics present in historical data [26]. This form of predictive modelling assumes that past patterns shape future behaviours, making it an indispensable tool in various fields, ranging from weather forecasting [27] to stock-market predictions [28].

While time-series modelling is a powerful tool for forecasting future data, it also has its challenges and limitations. Time-series data often exhibit seasonality and trends, which can complicate the forecasting process [29]. Outliers, missing sequences of data, and anomalies can also significantly impact the accuracy of forecasting models, requiring careful identification and handling. The capacity of these models to integrate external influential factors and variables is also somewhat limited, often necessitating the integration of additional features for enhanced predictive accuracy [30]. Additionally, time-series models require significantly more data for training, which can be cumbersome in situations where data are limited [30]. These challenges highlight the importance of adopting a methodical approach to time-series modelling, emphasising the need to carefully consider the specific context and characteristics of the data being analysed when utilising time-series models for effective forecasting.

In the context of this work, SSC velocities were predicted using time-series modelling. Accurate predictions require a detailed analysis of data sequences to discern patterns that could forecast future predictions. The historical hourly data of SSC form a time series, which is inherently continuous but sampled at discrete intervals. To address this, LSTM and GRU models are used due to their competence in handling vast amounts of sequential data and their capacity to learn complex temporal patterns [31–33]. After training on past SSC data, these models can predict future values with good accuracy.

2.4. Data Integration and Preprocessing

The raw data are split into multiple folders and sub-folders for each day, necessitating a robust method to merge and preprocess the data without interfering with their temporal and spatial dimensionality.

To address this, a utility was developed that allowed us to specify the start and end dates for the merging of the SSC data. This then merged the individual files along the time dimension, creating a single data set that encompassed all relevant data across the specified interval. This merged data set was not only more manageable but also streamlined for any subsequent processes. A key feature was the preservation of the geographical boundaries and temporal aspects of the data. The data set maintained the latitude and longitude ranges, ensuring that spatial integrity was uncompromised. Furthermore, checks were performed to ensure that the time remained consistent, preserving the temporal integrity of the data.

When the data were analysed, a substantial number of missing values, represented as *not-a-number* (NaN), were discovered. These NaNs were likely due to the proximity of the data to the coast, where high-frequency radars often struggle to capture all the data accurately. At this stage, NaN values were not addressed. Each objective required the tailored handling of missing data, which will be discussed in the next sections.

2.5. The Lagrangian Model's Development

Due to the strengths highlighted in Section 2.2, the OceanParcels toolkit [9] was chosen for this study. The first step was to create the land–sea mask, as can be seen in Figure 3. This effectively differentiates the land from the sea, ensuring accurate particle behaviour. The mask was saved as a NetCDF [16] file and added within the grid boundaries to match the boundaries of the data set. These coastal boundaries define the simulation area and facilitate land–sea interactions.
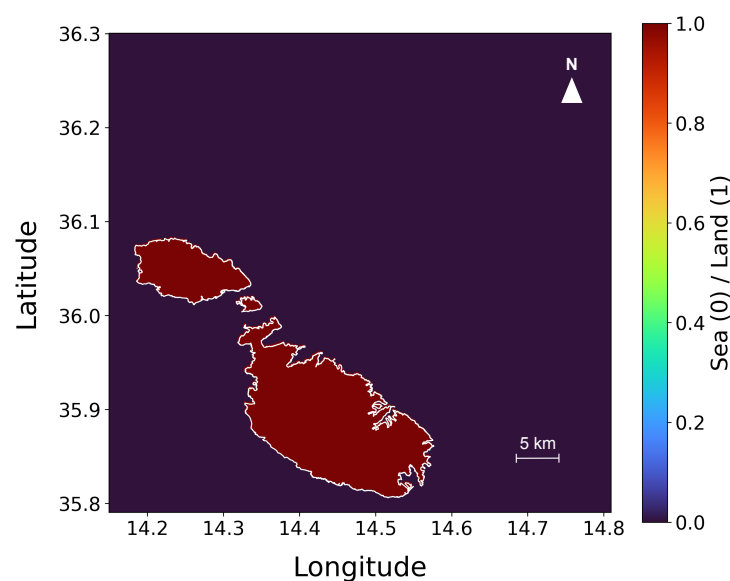

Figure 3. Land–sea mask of Malta.

Subsequently, a *FieldSet* was created from the SSC data set. This served as the simulation environment, defining the velocity fields that drive particle movement. Additionally, the land–sea mask was integrated into the *FieldSet*, providing necessary data for handling particles upon their reaching land. As depicted in Figure 4, simulation particles were initialised near a specific geographic coordinate (36.0475° N, 14.5417° E) with random offsets to simulate a dispersed release. The particles represent the objects of interest, such as sea-surface debris, whose movements were to be simulated. Initially, the strategy involved simulating numerous randomly placed particles across the entire area; however, to enhance realism, a cluster of 50 particles was placed in close proximity. This configuration was selected to accurately represent how debris navigates marine environments, with each particle representing a cluster of debris.
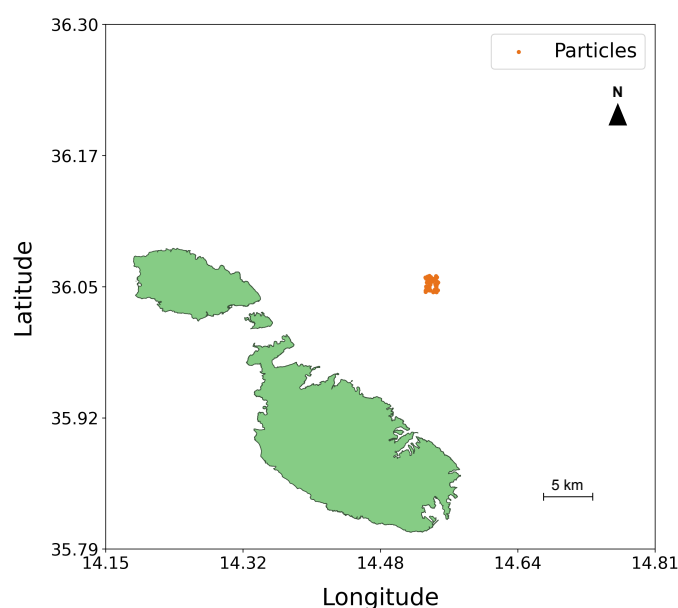
Figure 4. Location of initial particles showing a cluster of debris.

Custom kernels were a critical component of the simulation, and they allowed us to introduce specific behaviours into the simulation, thereby modelling realistic scenarios that particles may encounter. The behaviours implemented include the following:

- *Check out of Bounds,* which deletes particles from the simulation if they move beyond the defined boundaries. This is necessary because no data are available outside the boundary, causing particles to get stuck.
- *Check Error,* which deletes particles encountering computational errors. This ensures that the simulation proceeds without disrupted or incorrect particle data.
- *Update Elapsed Time*, which shows how long a particle has been in the simulation. This tracks the duration of the particle within the environment.
- *Update Previous Position,* which captures the positions of particles before they move. This is useful, as it allows us to save all the previous positions of the particles.
- *Reflect on Land,* which applies a reflection behaviour when particles encounter land, as defined by the land–sea mask. It also introduces a probabilistic component when there is a 15% chance that particles will 'beach' and be removed from the simulation, while the remaining 85% chance allows particles to be reflected back into the sea. This probabilistic distribution is justified by the geographic characteristics of Malta, where the predominance of rocky coastlines over sandy beaches increases the likelihood of debris being deflected back into the sea, rather than getting beached.

The simulation was executed, and the resulting particle movements and dispersion patterns were visualised. These visualisations provide valuable insights into the trajectories of particles and their interactions with the environment. The time-step for the Lagrangian

simulation was set to 10 min, capturing the continuous dynamics of particle dispersion. This interval provided a good balance between computational efficiency and accuracy. The results were saved as an animated GIF file, offering a dynamic and easily interpretable visual representation of the simulated particle dispersion over time.

Some challenges emerged during this part of the implementation. Initially, simulations revealed that particles were getting stuck at the border boundaries. This issue was traced back to the data set, which lacked data at the borders, rendering the particles unresponsive to environmental variables in these areas. To address this, the boundary of the simulation area was slightly reduced by 0.1° in longitude and latitude. The simulation was defined over a seven-day period (longer periods were unreasonable and did not align with the research goals). To achieve this, the preprocessing steps discussed in Section 2.4 were utilised to merge the data from 1st to 7th January 2023. Wind was not considered in the simulation, as the spatial distribution of microplastics does not appear to be significantly affected by it. This intuition is supported by the research done by M. Erikson et al. [34]. Despite this, it may still be possible that wind data may enhance the accuracy of the simulations in depicting real-life scenarios, and they may provide an interesting improvement.

To deal with the missing data, an attempt was made to interpolate the missing values. The visualisation results were noticeably different from those produced using the raw data which included NaNs. Despite experiments with both linear and spline interpolation, the outcomes of the interpolated simulations remained consistent across different time frames, suggesting that the interpolation excessively homogenised the data. This uniformity introduced via interpolation was misleading, as it failed to represent the true variability and dynamics of the SSC, compromising the actual behaviour and movement patterns of particles in the sea. Consequently, it was decided not to remove NaN values from the data used in the Lagrangian simulations. This decision was based on the understanding that removing or interpolating these values could lead to simulations that would not accurately reflect real-world conditions. Preserving the integrity of the original data set, including its inherent gaps, mean that the simulations were more likely to represent the actual conditions and variations that marine debris would encounter in the sea. Examples of the final visualisations are shown in Section 2.7.

2.6. Ml Model Selection

A pipeline was established to predict the SSC velocities. The initial phase involved selecting appropriate models, with LSTM and GRU architectures identified as the optimal choices. This decision was informed by their demonstrated effectiveness in processing time-series data, rendering them particularly suitable for this task, as shown in studies by A. M. Ali et al. [35] and I. I. Zulfa et al. [12]. Utilising these models allows the the dispersion of marine debris around Malta's coastal waters to be accurately predicted, addressing both the temporal dynamics and spatial complexities inherent to SSC movements.

2.6.1. Data Preprocessing and Geospatial Filtering

While the initial plan was to train a model on a year's worth of data in order to forecast SSC for the next month, the complexity and four-dimensional nature of the data led to sub-optimal predictions. Consequently, the strategy was revised to extend the data set used for training, which spanned from 25 February 2020 to 1 August 2023. Given the substantial volume of data points and the need for geospatial filtering, a decision was made to concentrate on a smaller area of interest along the northern coast of Malta, as illustrated in Figure 5. The method involved predicting the u and v components individually for each longitude-and-latitude pair within the defined area. These individual predictions were subsequently merged into a single file and finally input into the Lagrangian simulation.
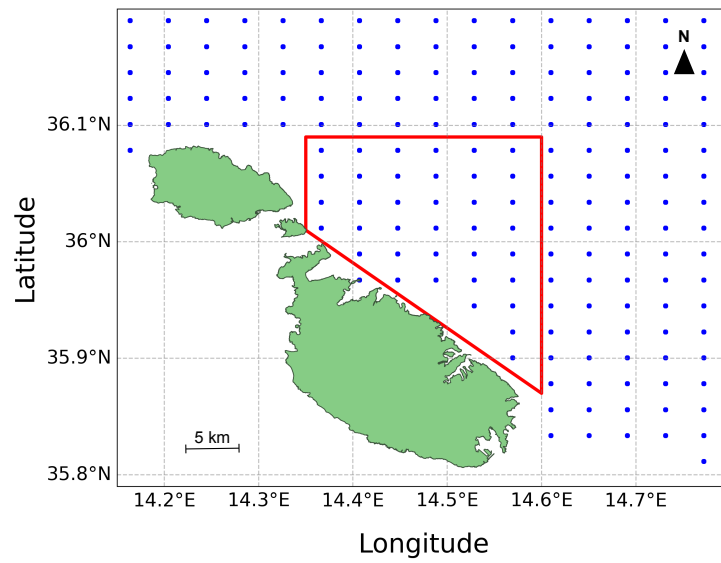
Figure 5. Data points and selected area of interest.

The data set was geospatially filtered to include only data points within the designated area of interest, as shown in Figure 6. This filtering resulted in a focused data set consisting of 37 data points. The data did not require any normalisation, as they had already been scaled between −1 and 1 during the data-collection phase. Each coordinate pair was then processed into individual comma-separated value (CSV) files. These files were systematically named and organised according to the corresponding latitude and longitude coordinate points. These CSV files served as the basis for training the AI models for every individual data-point location.
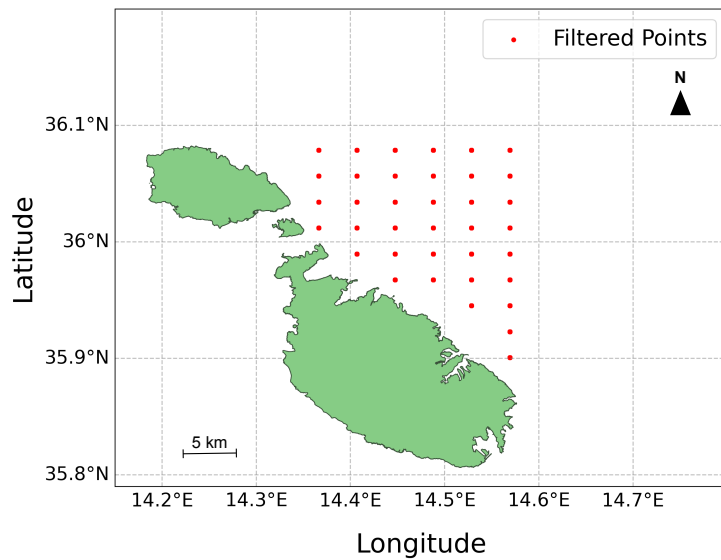

Figure 6. Filtered points within area of interest.

Areas closer to the coast had fewer data points (more NaNs), as illustrated in the heat map in Figure 7. This lack of data near coastal regions can likely be attributed to several factors. These include radar interference from nearby land or structures, the obstruction of radar beams due to coastal terrain or buildings, and the refraction of radar waves at the coast, all contributing to distorted data collection. Efforts to solve this issue included experiments with data interpolation and filling missing values with the mean. However, these methods yielded worse results compared to those obtained by eliminating the NaN values. Due to this, the most effective strategy proved to be the removal of NaN values,

a decision informed by testing and alignment with the methodologies applied for the Lagrangian model, as discussed in Section 2.5.
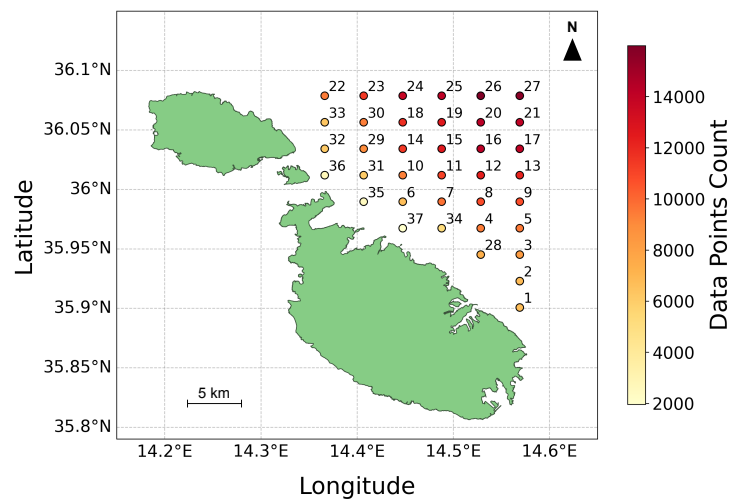
**Figure 7.** Amount of data points per coordinate pair.

Prior to creating the pipeline, preliminary testing was conducted on a single model to determine the most effective features and targets. Experimentation involved the integration of both *u* and *v* as features, revealing marginally improved outcomes compared to using each as a single feature, prompting a focus on using both features for the predictions. Notably, the model yielded good results when predicting a single target, but the accuracy of predictions noticeably diminished upon testing the model to predict both *u* and *v* as targets. This observation led to the decision to develop separate models for each target variable in order to maximise the accuracy of the results. Therefore, a series of 37 models to predict the *u* component was implemented and repeated similarly for the *v* component, ensuring precise and reliable predictions.

2.6.2. The Main Loop

Inspired by the approach of H.-M. Choi et al. [36], who developed a model for every individual coordinate pair, a pipeline was established that iterated through each pair of coordinates in the data set (total of 37) and trained a dedicated model for each individual pair. This approach made possible predictions across the entire area of interest, which were later utilised for the Lagrangian simulations. The *u* and *v* columns in the data files prepared earlier were extracted as input features. The data set was then divided into training, validation, and testing sets in a 70-15-15 split, respectively, a common split for ensuring a balance between adequate model training and thorough evaluation. Given the time-series nature of the data, it was necessary to sequence the data appropriately; this was achieved using the *TimeseriesGenerator* library [37]. The iterative testing of different parameter combinations revealed that a window size of 72 h, a batch size of 64, and a sampling rate of 1 unit yielded the best overall results. This meant that the data were sequenced into continuous blocks of 72 h of data as input and paired with the value immediately following these 72 h as the target output. This step allowed the model to predict the next hour based on the preceding 72 h of data.

TensorFlow [38] was used to implement the models. Various architectures and hyperparameters were tested to determine which ones yielded the best results, including a partial grid search for hyperparameter tuning. To ensure a fair comparison, identical hyperparameters and layer configurations were applied across both the LSTM and GRU architectures. The most effective architecture involved ten hidden layers, composed of four LSTM/GRU layers, three dropout layers, and two dense layers activated via *ReLU*, followed by an additional dropout layer after each dense layer. The models were set up

with a learning rate of 0.001, the *ADAM* optimiser, and the MSE loss function. Importantly, the model was reinitialised in each iteration of the loop, ensuring that each data set was trained on a fresh instance without any residual weights from previous iterations. This approach is crucial when dealing with multiple data sets to avoid any data leakage or influence from previously trained models (clean-slate training). It also helps maintain the integrity of the learning process for each distinct data set. Early stopping with a patience of 8 epochs was implemented to halt training and prevent overfitting. Model checkpoints were utilised to save the best-performing epoch automatically. After each training epoch, plots comparing training versus validation loss were generated to monitor the performance of each model. To ensure that each model was trained adequately, predictions were made on the test set and subsequently visualised by comparing actual versus predicted values, as illustrated in Figure 8. Finally, in the adoption of a similar evaluation approach to Adhikari et al. [25], MAE, MSE, and RMSE error metrics were computed and displayed to evaluate the model's performance using the test set.
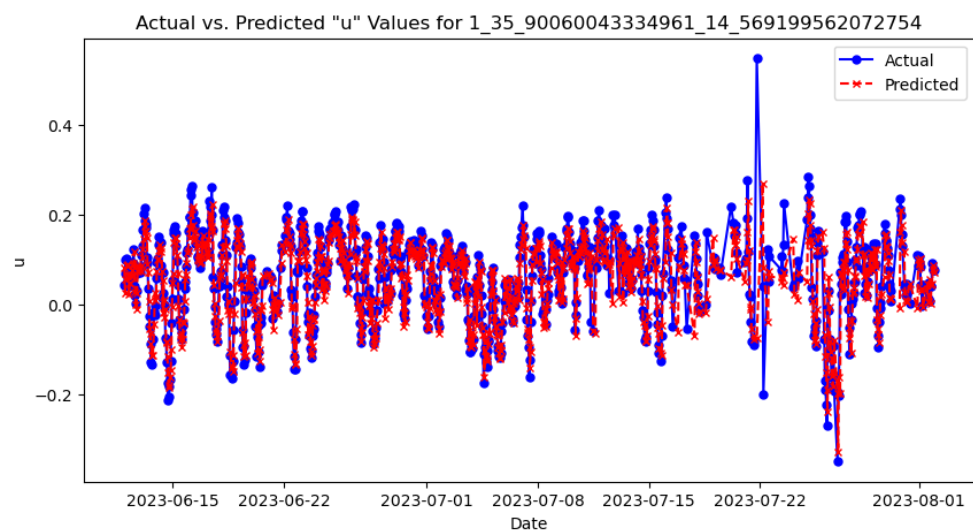
Figure 8. Actual vs. predicted values using the test set.

2.6.3. Making Real-World Predictions

In the final phase of the AI model pipeline, a simulation mirroring a real-world scenario was made by feeding historical data spanning 72 h to predict the subsequent 24 h. This 24-h prediction window was chosen since it provides a balance between short-term accuracy and computational feasibility, which is typically used for time-series forecasting in dynamic environments like SSC. The dates of 4th August and 4th November 2023 were selected to assess the model's performance under different seasonal conditions; from here on, they are referred to as *Test 1* and *Test 2*, respectively. Specifically, data from 1st to 3rd August 2023 were used as input to predict conditions for *Test 1*; data from 1st to 3rd November were used for *Test 2*. This setup allowed us to compare the predictions with actual historical data from the data set. The process began with a loop to systematically extract SSC data across 72 h for all 37 individual coordinate pairs. Subsequently, actual observed data for the following 24-h period on 4th August (*Test 1*) were extracted for comparative purposes, and both sets were saved as CSV files. Given the requirement for 72 consecutive hours of data to be able to make predictions and 24 h for comparison, spline interpolation was utilised to address any present NaN values, ensuring the data set's completeness (this is distinct from the case in which NaNs were ignored as discussed in Section 2.5). Using the rolling forecasting method shown in Figure 9, predictions were generated for the subsequent 24-h period for the individual targets *u* and *v*. It is noted that predictions based on interpolated data served as inputs for subsequent forecasts, potentially diminishing their precision. This effect was particularly noticeable in longer-term predictions, for which accuracy tended to

decrease as the forecast horizon was extended, expectedly showing a decline in prediction accuracy the farther the prediction extended into the future.
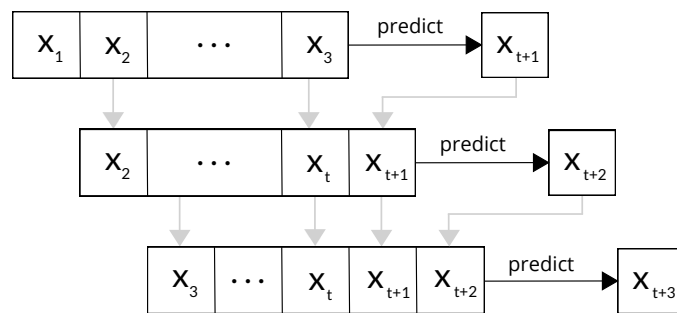

Figure 9. The process of a rolling forecast.

This process was repeated for all 37 data points, and the predictions were converted into the NetCDF format to be subsequently used in the Lagrangian model. Finally, the same error metrics were calculated to be used later for evaluation. This pipeline was repeated four times, encompassing two LSTM models and two GRU models, one for each of the *u* and *v* components, respectively. The architecture of the AI models' pipeline is illustrated in Figure 10 below.
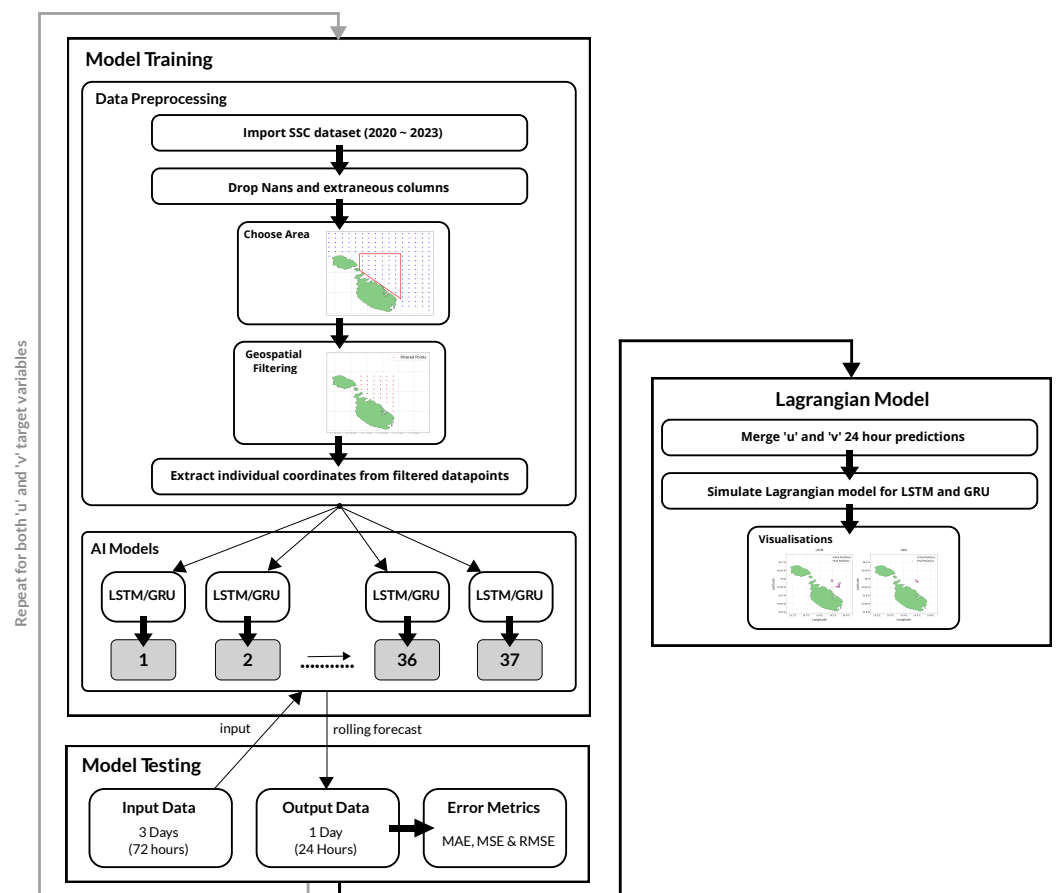

Figure 10. Overview of the entire pipeline.

### 2.7. Integrating the ML Models with the Lagrangian Model

The final stage of the pipeline involved integrating the AI models' predictions with the physics-based Lagrangian model to produce a 24-h forecast simulation of sea-surface debris dispersion.

This process was conducted separately for both the LSTM and GRU model predictions. The initial and most critical step involved the preprocessing and merging of the predicted *u* and *v* values as NetCDF data. Following this, the procedures outlined in Section 2.5 were implemented once again to set up the Lagrangian simulation framework. This involved the configuration of the land–sea mask, *FieldSet*, number of particles, kernels, and timestep. The only difference lay in the particle-initialisation phase. Given that the model predictions were specific to the area of interest (as depicted in Figure 6), it was decided to set the centroid of the polygon as the starting position. More specifically, the coordinates were at a latitude of 35.9895° and a longitude of 14.4944°. This approach is advantageous, as it allows for an unbiased observation of dispersion patterns. The reason is that, since the centroid is equidistant from all edges of the polygon, it provides a neutral starting point that does not inherently favour any flow direction. In terms of the offset of the initial particles, the same random seed was used for both the LSTM and GRU simulations. This ensured a fair comparison, as the initial locations of the particles were identical for both models.

Finally, the Lagrangian simulations for both the LSTM and GRU models were executed and stored. The resulting particle movements and dispersion patterns were visualised. These visualisations (Figures 11 and 12) allowed us to observe the surface-debris movement predictions and facilitate the evaluation of the results produced via the LSTM and GRU models.
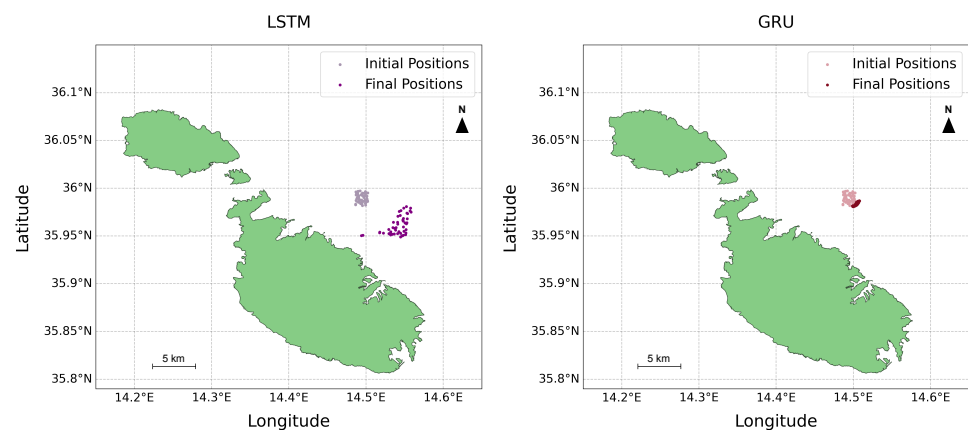
Figure 11. LSTM and GRU initial vs. final debris movement for *Test 1* (4th August).
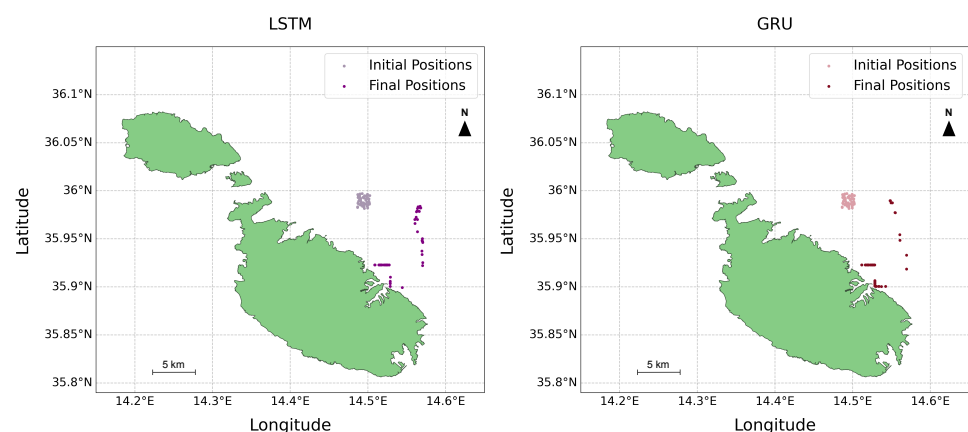
Figure 12. LSTM and LSTM initial vs. final debris movement for *Test 2* (4th November).

2.8. Evaluation Strategy

The original plan was to evaluate the Lagrangian framework by comparing dispersion patterns with drifter data, as done by van Sebille et al. [6] and Aijaz et al. [39]. However, due to the coastal proximity of the area of interest and the general practice of deploying drifters in open waters to avoid beaching, the drifter trajectory data were not available. While

this would be the ideal approach to assessing the Lagrangian simulations, this proved to be impossible due to the unavailability of drifter data. Instead, the focus shifted to the analysis of the LSTM and GRU model predictions. Through the adoption of an approach similar to that of H. Yadav et al. [40], the mean absolute error (MAE), mean squared error (MSE), and root mean squared error (RMSE) were used to assess their predictive accuracy. Furthermore, to ensure that the procedure could generalise well, it was also run on the *Test 2* timeframe (in a different season) from the 1st to the 3rd November 2023 using the same trained models.

Given that this analysis included 37 distinct models for both the *u* and *v* components, the mean and standard deviation were computed for each metric to facilitate a more comprehensive evaluation of the LSTM and GRU. During the analysis, certain outliers within the results were identified. To address this, the average was also calculated using the interquartile range (IQR), focusing on the differences between the 75th and 25th percentiles for each metric and thereby obtaining a more robust mean that excluded these outliers.

A geospatial evaluation of the LSTM and GRU models was motivated by the observation that each specific data point within the area of interest yielded varied results. Initially, a heat map was generated (Figure 7) to identify which model corresponded to each location and to quantify the amount of training data available for each model. Subsequently, the MAE values for the *u* and *v* components were visualised again using heat maps. The choice of MAE as a metric was deliberate, as it provides a straightforward and uniformly interpretable measure that treats all errors equivalently. These visualisations were instrumental in comparing the spatial accuracy of the models, highlighting areas where each model exhibited better or worse performance. These findings were then compared with the original heat map to discern patterns and discrepancies. This analysis was performed for the predictions corresponding to both *Test 1* and *Test 2*.

Finally, the performance of the LSTM and GRU models was quantified across different regions, calculating the centroid, spread, and skewness of their respective Lagrangian simulation outputs. The measures included the following:

- Mean, median, and standard deviation of centroids: the geographical centroids of the merged predictions were computed from both the LSTM and GRU models to assess the proximity of the final debris-movement predictions generated via the two models. Smaller mean, median, and standard deviation values suggested a higher degree of consistency between the models' predictions.
- Spread of LSTM and GRU: the spatial spread was determined by calculating the standard deviation of distances from each model's centroid. A lower standard deviation indicated a tighter clustering around the centroid, reflecting more consistent model performance across the area.
- Longitudinal and latitudinal skewness of LSTM and GRU: to understand the directional tendencies of the model's predictions, the skewness of the distribution of the prediction points' longitude and latitude was calculated. A skewness close to zero indicates a symmetrical distribution of prediction errors, whereas a positive or negative skewness value points to a systematic bias in a particular direction.

3. Results

The primary objectives were to ascertain which model (LSTM or GRU) demonstrated superior performance and to evaluate the real-world similarity of the Lagrangian simulations generated using these models' predictions. As previously noted, the framework was tested on two time periods. This was done to gauge the models' consistency and reliability under varying seasonal conditions, offering a thorough analysis of their performance across different environmental dynamics.

3.1. LSTM vs. GRU

In the initial experiment, the accuracy of the models in predicting SSC velocities was assessed by comparing the predicted results against actual historical values using the MAE, MSE, and RMSE metrics.

Error Metric Results

The average error metrics for the 24-h rolling predictions from all 37 models in *Test 1* are presented in Tables 1–4 below.

Table 1. LSTM *u* average error metrics for *Test 1* (4th August).

Metric	Mean	Std. Dev.	IQR
MAE	0.141	0.226	0.058
MSE	0.116	0.513	0.010
RMSE	0.179	0.291	0.053

Table 2. LSTM *v* average error metrics for *Test 1* (4th August).

Metric	Mean	Std. Dev.	IQR
MAE	0.144	0.134	0.141
MSE	0.064	0.109	0.073
RMSE	0.183	0.175	0.212

Table 3. GRU *u* average error metrics for *Test 1* (4th August).

Metric	Mean	Std. Dev.	IQR
MAE	0.148	0.222	0.067
MSE	0.116	0.503	0.016
RMSE	0.187	0.285	0.070

Table 4. GRU *v* average error metrics for *Test 1* (4th August).

Metric	Mean	Std. Dev.	IQR
MAE	0.145	0.138	0.149
MSE	0.066	0.112	0.066
RMSE	0.184	0.179	0.202

The analysis of these results revealed insightful differences in model performance. For the *u* component, the LSTM models demonstrated slightly lower MAEs and RMSEs, indicating better average accuracy and consistency, although the GRU models showed a marginally lower MSE. Conversely, for the *v* component, both models performed similarly, with minimal variations across all metrics, which suggests a near-equivalent capability in handling this type of prediction. A further examination of the variability through standard deviation and IQR metrics showed that the LSTM models had a lower standard deviation in the *v*-component predictions, suggesting more consistent performance relative to GRU. Additionally, the smaller IQR for LSTM in both components implies that its predictions were more tightly clustered around the median, indicating less variability and more reliability. While both models performed well, LSTM offered marginally better performance, particularly for the *u* component, establishing it as the preferable model.

The results for the 24-h rolling predictions for all 37 models in *Test 2* are detailed in Tables 5–8 below.

Table 5. LSTM *u* average error metrics for *Test 2* (4th November).

Metric	Mean	Std. Dev.	IQR
MAE	1.031	2.118	0.299
MSE	14.765	40.758	0.243
RMSE	1.634	3.478	0.397

Table 6. LSTM *v* average error metrics for *Test 2* (4th November).

Metric	Mean	Std. Dev.	IQR
MAE	2.622	5.507	0.506
MSE	97.858	253.429	0.860
RMSE	4.239	8.938	0.844

Table 7. GRU *u* average error metrics for *Test 2* (4th November).

Metric	Mean	Std. Dev.	IQR
MAE	1.051	2.112	0.568
MSE	14.772	40.773	0.466
RMSE	1.651	3.471	0.586

Table 8. GRU *v* average error metrics for *Test 2* (4th November).

Metric	Mean	Std. Dev.	IQR
MAE	2.653	5.502	0.537
MSE	97.980	253.623	1.144
RMSE	4.268	8.931	0.991

When it comes to the *u* component, both models displayed relatively high MAEs, MSEs, and RMSEs, with LSTM showing lower metrics. The high standard deviations observed for both models suggest a significant presence of outliers, indicating that some predictions were inaccurate. This is evident in the GRU *u* component, for which the IQR was higher, suggesting a broader spread compared to LSTM and pointing to more frequent outliers in the GRU model. In contrast, the *v* component exhibited considerably higher error values for both models, with GRU again having higher values across all metrics. The standard deviations and IQR values were significantly larger in the *v* component for both models, again reinforcing the presence of outliers and indicating that predictions for the *v* component were generally less accurate and more variable. Overall, the LSTM model performed better than the GRU model, particularly with the *v* component, as evidenced by the lower error metrics and narrower IQR. Therefore, the more consistent performance of LSTM across both tests seems to suggest that it is the better model overall.

4. Discussion

4.1. Error Metric Results

The analysis highlighted that predictions of the *u* component (east–west velocity) were generally more accurate than for the *v* component (north–south velocity). This discrepancy can be attributed to the baseline alignment of radar systems, which are aligned along a north–south orientation, as depicted in Figure 1. This potentially impacts the accuracy of *v*-component readings and inhibits the radar's ability to capture detailed north–south data, consequently leading to less accurate predictions for the *v* component. Moreover, *Test 1*, conducted on the 4th of August, exhibited notably better results, characterised by lower error values and fewer outliers when compared to *Test 2* on the 4th November. This improvement was likely due to the August data being in close proximity to the final sequences of the test data set, potentially leading to the models being better tuned to these

conditions. Furthermore, the process of rolling forecasting, which bases predictions on preceding outputs, may lead to inaccuracies, particularly when initial predictions are derived from interpolated data. This method could inherently propagate errors, especially under conditions of notable missing data, as discussed in Section 2.6.3. Such findings emphasise the necessity of considering temporal proximity and data integrity when assessing model performance. These phenomena and their implications on model performance will be explored further in the next section.

4.2. Geospatial Analysis

Another test focused on determining whether an increased volume of data correlated with enhanced predictive accuracy, whether data points closer to the coast, typically characterised by fewer data, yielded poorer performance, and whether the time of year and seasonality of the data impacted the results. The primary goal was to assess whether the geographical location of data points influenced the accuracy of the predictive models. Additionally, the final Lagrangian simulations generated via both the LSTM and GRU models were compared to evaluate their similarities in modelling sea-surface debris.

4.2.1. A Hypothesis

As highlighted in Sections 2.6.1 and 2.8, the data set contained considerable missing data, with data points closer to the coast having more NaNs present, as evidenced in Figure 7. This is corroborated by Figure 13, which illustrates how some data points had significantly less data available. Figure 7 is instrumental in demonstrating the correlation between model performance and geographic location, thereby paving the way for a focused analysis of the impact of data availability at specific locations. Based on these observations, a hypothesis was formulated.

Hypothesis 1. *Data points near the coast exhibit reduced data availability due to environmental and technical challenges that interfere with radar performance. This scarcity of data consequently impairs the accuracy of predictive models for SSC velocities near the coast. Specifically, it suggests that models predicting SSC at coastal locations perform less effectively compared to those further offshore, for which radar data tends to be more complete.*
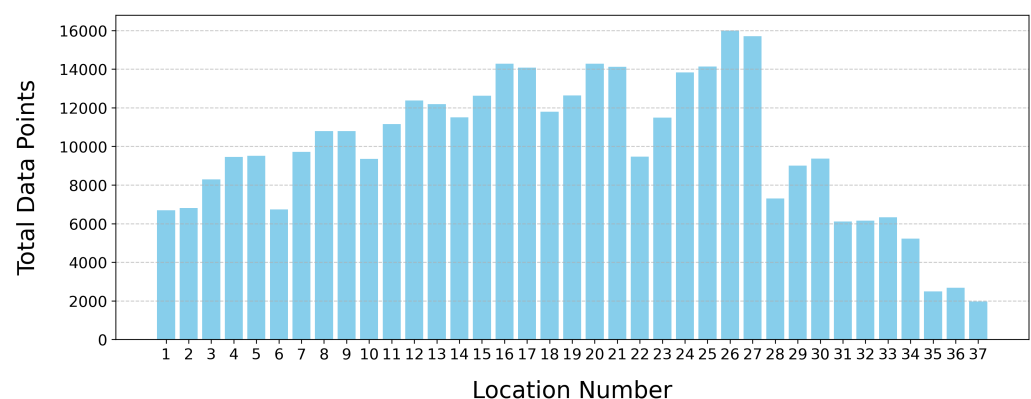
Figure 13. Histogram of data points by location number.

The hypothesis was investigated by conducting a comparative analysis with the heat map in Figure 7. This analysis helped us validate or refute the assumption regarding the influence of geographical location on model accuracy.

4.2.2. Heat Map Results and Analysis

As discussed in Section 2.8, heat maps were utilised to geospatially analyse the performance of the models, focusing on the MAE across all 37 models. These visualisations were crucial for testing the validity of the hypothesis regarding the impact of data availability on

predictive accuracy near coastal areas. Heat maps for the MAE metrics were produced for both the *u* and *v* components of both the LSTM and GRU models, covering the predictions made in both *Test 1* and *Test 2*. To enhance the clarity of these visualisations and minimise the influence of outliers, a clipping method was applied at the 95th percentile of the data. This method effectively limited the range of data considered for colour scaling in the heat maps, allowing for more nuanced visual comparisons between most data points by excluding extreme outliers. The resultant heat maps for *Test 1* are displayed in Figures 14 and 15, and the ones for *Test 2* are displayed in Figures 16 and 17 below.
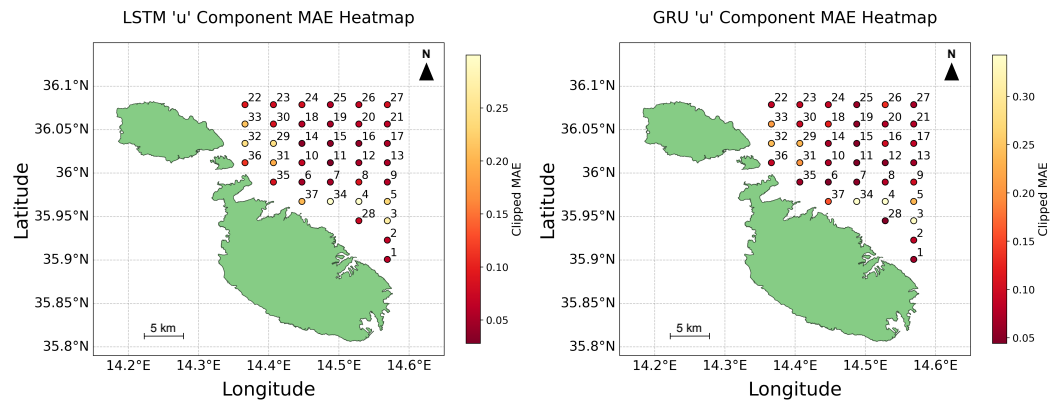

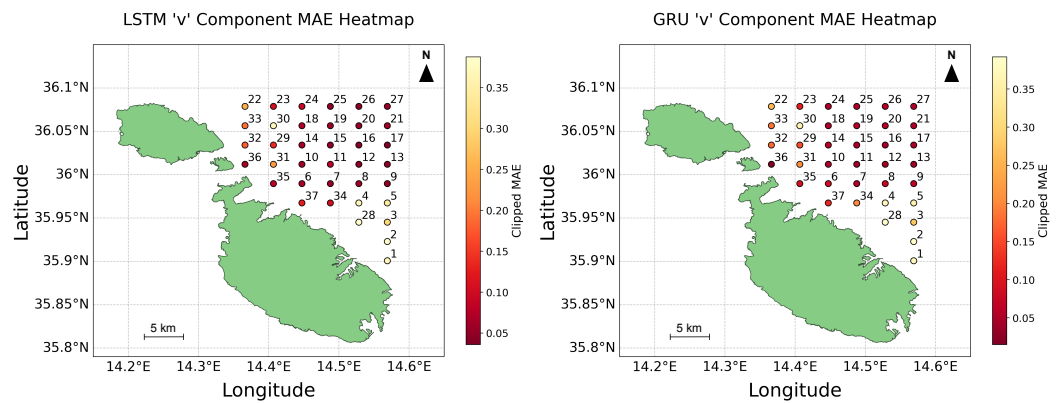**Figure 14.** *u* component MAE heat maps for *Test 1* (4th August).

Figure 15. *v* component MAE heat maps for *Test 1* (4th August).
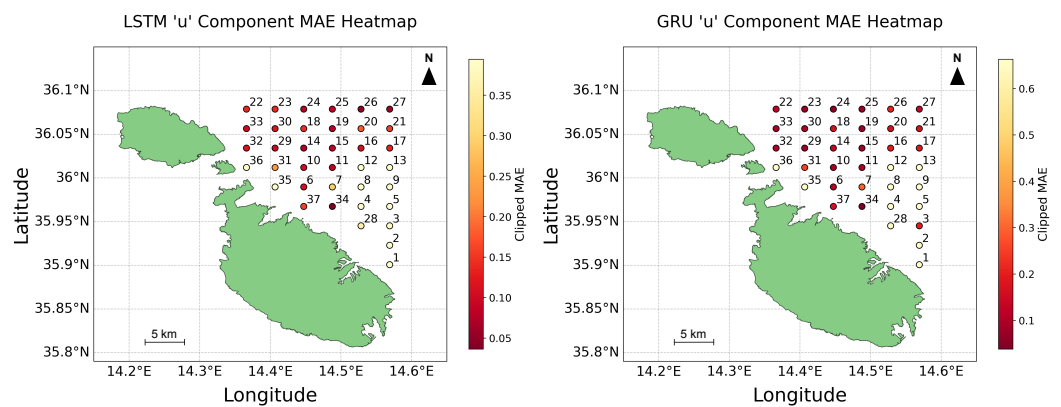

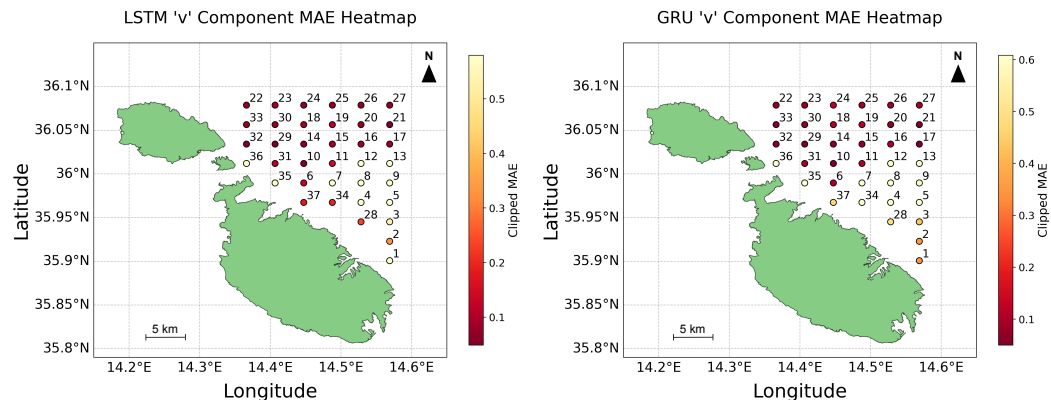**Figure 16.** *u* component MAE heat maps for *Test 2* (4th November).

Figure 17. *v* component MAE heat maps for *Test 2* (4th November).

These visualisations clarify that, while models near the coast generally performed worse, presumably due to fewer data being available, there were notable exceptions in which coastal predictions maintained good accuracy. This observation challenges the assumption that a greater data volume directly correlates with higher predictive accuracy. Instead, it suggests that the models' capabilities to handle noise and extract meaningful patterns from sparse data can significantly impact their effectiveness. Furthermore, the differential accuracy between the *u* and *v* components highlights the complexity of environmental factors and model sensitivities, which contribute to a diverse spectrum of outcomes that are not determined solely by the amount of data available.

Comparing the results obtained via the two tests revealed a stark contrast: the predictions for August were markedly more accurate, underscoring the potential impact of seasonal variations. The outliers observed in *Test 1* were inconsistent with those of *Test 2*, highlighting the temporal variability of missing data and its non-uniform impact across different points and times. It becomes evident that no consistent pattern existed, thus challenging any definitive conclusions. While certain models excelled in predicting the *u* component, their performance diminished when they were applied to the *v* component. These observations attest to the intricate dynamics at play in predictive modelling, where factors like the models' ability to manage noise and the inherent directional properties of data lead to outcomes in which fewer data does not always result in less accuracy. Therefore, these findings not only challenge but also effectively refute the hypothesis.

4.2.3. Comparison of Lagrangian Simulations

In the final component of the evaluation framework, the performance similarities between the LSTM and GRU models were assesed through the analysis of centroids, spreads, and skewness within the respective Lagrangian simulation outputs. The findings for *Test 1* are shown in Figure 18.

```
Mean Centroid Distance: 0.0196° (2.17 km)
Median Centroid Distance: 0.0186° (2.06 km)
Std Dev of Centroid Distances: 0.0138° (1.54 km)

LSTM Spread: 0.0163° (1.81 km)
GRU Spread: 0.0049° (0.54 km)

LSTM Longitude Skewness: 0.249
LSTM Latitude Skewness: -0.487
GRU Longitude Skewness: -1.076
GRU Latitude Skewness: 0.381
```

Figure 18. LSTM vs. GRU comparison of Lagrangian simulations for *Test 1* (4th August).

In this case, the average centroid distances for the LSTM and GRU models were around 2 km, suggesting that both models achieved markedly different geographical accuracy. The standard deviation of these distances was 1.54 km, indicating a moderate spread

around the centroids. However, the GRU model demonstrated a more compact spread of 0.54 km compared to the LSTM's 1.81 km, suggesting that GRU's predictions were more tightly grouped. The skewness metrics showed a mild eastward and southward bias in the LSTM predictions, whereas the GRU exhibited a stronger westward bias and a slight northward tendency, highlighting directional tendencies in their prediction patterns. Next, the results for *Test 2* are shown in Figure 19.

```
Mean Centroid Distance: 0.0147° (1.63 km)
Median Centroid Distance: 0.0172° (1.91 km)
Std Dev of Centroid Distances: 0.0063° (0.70 km)

LSTM Spread: 0.0144° (1.60 km)
GRU Spread: 0.0232° (2.58 km)

LSTM Longitude Skewness: 0.563
LSTM Latitude Skewness: -0.167
GRU Longitude Skewness: 0.278
GRU Latitude Skewness: 0.475
```

Figure 19. LSTM vs. GRU comparison of Lagrangian simulations for *Test 2* (4th November).

The results of the second test showed improvements in clustering, with mean and median centroid distances reduced to approximately 1.63 km and 1.91 km, respectively. This reduction, coupled with a decreased standard deviation of 0.70 km, suggests enhanced prediction accuracy and consistency for this period. Interestingly, LSTM showed a more consistent spread of 1.60 km, whereas GRU's predictions were more dispersed, with a spread of 2.58 km. Skewness values also shifted, indicating changes in predictive behaviour that might have been influenced by different environmental conditions or model sensitivities to the input data at that time.

Overall, the analyses highlight that the LSTM models generally offered more consistent and reliable performance, marked by less variability in spread and skewness compared to GRUs. While GRUs seemed to adjust their performance based on different conditions, suggesting a possible sensitivity to seasonal or environmental changes, the LSTM models maintained steadiness across the evaluated metrics. This consistent performance makes LSTM the more suitable model for this application.

4.2.4. Comparison of Final Lagrangian Visualisations

Visual comparisons between Figures 11 and 12 indicate notable differences in the outcomes of the LSTM and GRU simulations. Specifically, the August simulations (Figure 11) revealed distinct disparities in the final particle locations between the LSTM and GRU models. Conversely, the November simulations (Figure 12) displayed a high degree of similarity. This observation lends support to findings from our previous observations in Section 4.2.3, where the November results demonstrated greater alignment between the models when compared to August. Such disparities point out the variable nature of these predictions and highlight the complex interplay of various factors that significantly impact the accuracy and consistency of the final outcomes. This variability is illustrative of the inherent challenges in modelling time-series data, for which slight variations in input or parameters can lead to markedly different predictions.

5. Conclusions

In this study, an integrated system that combined ML models with a physics-based Lagrangian framework to forecast the movement and dispersion of sea-surface debris around Malta were proposed. The results demonstrate the capability of the system to make accurate 24-h predictions and dynamically visualise the trajectory of marine debris. Through a comparative evaluation, it was determined that the LSTM model outperformed the GRU model in predicting SSC velocities, evidenced by better performance in error metrics such as the mean absolute error (MAE), mean squared error (MSE), and root mean

squared error (RMSE). These findings validate the effectiveness of the integrated approach and demonstrate its potential to enhance marine conservation efforts.

The analysis consisted of an evaluation of error metrics and geospatial behaviour, which together provided a robust evaluation of the effectiveness of the models and the corresponding practical applicability. The findings indicate that LSTM provided more consistent and reliable predictions, establishing it as the preferred model when considering the performance of both components across diverse seasonal and environmental conditions. The geospatial analysis further corroborated these findings, showing that the LSTM generally maintained more consistent performance metrics, such as spread and skewness, when compared to the GRU. This consistency was evident despite the seasonal variations between the two dates, highlighting LSTM's robustness across different predictive scenarios.

Furthermore, this analysis did not consistently support the hypothesis that proximity to the coast and reduced data availability significantly degraded the models' performance. While coastal data points generally showed less accuracy, this was not universally the case. Some predictions maintained good accuracy, suggesting that other factors, such as the capacity of the models to handle sparse data and environmental noise, play a critical role in prediction outcomes. Therefore, the findings do not support the hypothesis that fewer data inherently results in poorer model performance.

Throughout this study, several challenges and limitations were encountered. The primary challenge was the presence of missing data, particularly near coastal areas, which likely affected the precision of the two predictive models. Moreover, the geographical area of interest was limited, potentially constraining the broader applicability of these findings. The final limitation was the inability to empirically validate the Lagrangian model due to the absence of drifter data within the chosen area.

Integrating additional weather parameters, such as wind and wave action into the models to enhance the predictions, is left as future work. Additionally, the framework can be adapted to various applications, including jellyfish and plankton movements, search and rescue operations, and oil-spill trajectory simulations. Further enhancements in predictive accuracy could be achieved by implementing ensemble learning methods, as evidenced by the research of B. Naderalvojoud and T. Hernandez-Boussard [41], and by integrating more sophisticated models such as transformers [42]. Expanding the area of interest could provide a more comprehensive understanding of marine debris dynamics while also enabling the evaluation of the Lagrangian model using historical drifter data. Implementing a model specifically designed to predict and fill in missing values within the data sets could enhance the accuracy of predictions and improve visualisations. Finally, developing a front end to display future predictions with enhanced visualisations would make the research more accessible, allowing interaction with the data in real time and fostering greater engagement with and understanding of the capabilities of the model and environmental implications.

In Malta, there is a significant issue of litter on the beaches, particularly microplastics. Some beaches experience higher levels of contamination than others, and there is uncertainty about whether the influx of plastics originates from land-based sources or the sea. Eventually, this study aims to analyse these patterns and identify the sources of beach litter, providing critical information for targeted clean-up efforts and policy-making. Additionally, the Malta Channel is a heavily trafficked maritime route with numerous cargo ships passing through. This research can help identify potential hotspots for litter accumulation, which is crucial in the event of a spill or accident. Understanding these hotspots will enable more effective response strategies for mitigating environmental damage. Moreover, this study serves as foundational work for a jellyfish dispersion model. This future model will allow us to predict the spread of jellyfish blooms and determine which bays will be affected. Such information is vital for public safety, tourism, and marine ecosystem management. While these applications are indeed practical and highly useful, they are beyond the scope of the current paper. Here, a model has been presented that was specifically configured

and optimised for analysing floating litter, laying the groundwork for future research in these areas.

Author Contributions: Conceptualisation: M.D., A.G. and K.G.; methodology: M.D. and K.G.; investigation: M.D. and K.G.; data set: A.G.; evaluation: M.D.; analysis: M.D. and K.G.; writing—original draft: M.D. and K.G.; writing—review and editing: M.D., A.G. and K.G.; project administration: K.G. All authors have read and agreed to the published version of the manuscript.

Data Availability Statement: The source code and data sets used in this study are publicly accessible on GitHub (https://github.com/markdingli18/FYP_Mark_Dingli, accessed on 29 August 2024).

Abbreviations

The following abbreviations are used in this manuscript:

AI	Artificial intelligence
ANN	Artificial neural network
GRU	Gated recurrent unit
IQR	Interquartile range
LSTM	Long short-term memory
MAE	Mean absolute error
ML	Machine learning
MSE	Mean squared error
NetCDF	Network Common Data Form
NaN	Not-a-number
RNN	Recurrent neural network
RMSE	Root mean squared error
CSV	Comma-separated value
SSC	Sea-surface current

References

1. Suaria, G.; Aliani, S. Floating debris in the Mediterranean Sea. *Mar. Pollut. Bull.* **2014**, *86*, 494–504. [CrossRef] [PubMed]
2. Compa, M.; Alomar, C.; Wilcox, C.; van Sebille, E.; Lebreton, L.; Hardesty, B.D.; Deudero, S. Risk assessment of plastic pollution on marine diversity in the Mediterranean Sea. *Sci. Total Environ.* **2019**, *678*, 188–196. [CrossRef] [PubMed]
3. Laist, D.W. *Impacts of Marine Debris: Entanglement of Marine Life in Marine Debris Including a Comprehensive List of Species with Entanglement and Ingestion Records*; Marine Debris: Sources, Impacts, and Solutions; Springer: New York, NY, USA, 1997; pp. 99–139. [CrossRef]
4. Rochman, C.M.; Browne, M.A.; Underwood, A.J.; van Franeker, J.A.; Thompson, R.C.; Amaral-Zettler, L.A. The ecological impacts of marine debris: Unraveling the demonstrated evidence from what is perceived. *Ecology* **2016**, *97*, 302–312. [CrossRef] [PubMed]
5. Agamuthu, P.; Mehran, S.B.; Norkhairah, A.; Norkhairiyah, A. Marine debris: A review of impacts and global initiatives. *Waste Manag. Res.* **2019**, *37*, 987–1002. [CrossRef] [PubMed]
6. Van Sebille, E.; Aliani, S.; Law, K.L.; Maximenko, N.; Alsina, J.M.; Bagaev, A.; Bergmann, M.; Chapron, B.; Chubarenko, I.; Cózar, A.; et al. The physical oceanography of the transport of floating marine debris. *Environ. Res. Lett.* **2020**, *15*, 23003–23032. [CrossRef]
7. Hardesty, B.D.; Harari, J.; Isobe, A.; Lebreton, L.; Maximenko, N.; Potemra, J.; van Sebille, E.; Vethaak, A.D.; Wilcox, C. Using Numerical Model Simulations to Improve the Understanding of Micro-plastic Distribution and Pathways in the Marine Environment. *Front. Mar. Sci.* **2017**, *4*, 30. [CrossRef]
8. Winans, W.R.; Chen, Q.; Qiang, Y.; Franklin, E.C. Large-area automatic detection of shoreline stranded marine debris using deep learning. *Int. J. Appl. Earth Obs. Geoinf.* **2023**, *124*, 103515. [CrossRef]
9. OceanParcels. Available online: https://oceanparcels.org (accessed on 27 March 2024).
10. Yuniarti, M.; Faid, G.M.; Subiyanto; Ismail, M.R. Trajectory mapping of microplastics originating from the Seto Inland Sea, Japan. *AACL Bioflux* **2023**, *16*, 3138–3149.
11. Kehl, C.; Nooteboom, P.D.; Kaandorp, M.L.A.; van Sebille, E. Efficiently simulating Lagrangian particles in large-scale ocean flows—Data structures and their impact on geophysical applications. *Comput. Geosci.* **2023**, *175*, 105322. [CrossRef]
12. Zulfa, I.I.; Novitasari, D.C.R.; Setiawan, F.; Fanani, A.; Hafiyusholeh, M. Prediction of Sea Surface Current Velocity and Direction Using LSTM. *Indones. J. Electron. Instrum. Syst.* **2021**, *11*, 93–102. [CrossRef]

13. Mansui, J.; Darmon, G.; Ballerini, T.; van Canneyt, O.; Ourmieres, Y.; Miaud, C. Predicting marine litter accumulation patterns in the Mediterranean basin: Spatio-temporal variability and comparison with empirical data. *Prog. Oceanogr.* **2020**, *182*, 102268. [CrossRef]

14. Ryan, P.G. *A Brief History of Marine Litter Research; Marine Anthropogenic Litter*; Springer International Publishing: Cham, Switzerland, 2015; pp. 1–25. [CrossRef]

15. Harlan, J.; Terrill, E.; Hazard, L.; Keen, C.; Barrick, D.; Whelan, C.; Howden, S.; Kohut, J. The Integrated Ocean Observing System High-Frequency Radar Network: Status and Local, Regional, and National Applications. *Mar. Technol. Soc. J.* **2010**, *44*, 122–132. [CrossRef]

16. UNIDATA | NETCDF. Available online: https://www.unidata.ucar.edu/software/netcdf/ (accessed on 14 March 2024).

17. Van Sebille, E.; Griffies, S.M.; Abernathey, R.; Adams, T.P.; Berloff, P.; Biastoch, A.; Blanke, B.; Chassignet, E.P.; Cheng, Y.; Cotter, C.J.; et al. Lagrangian ocean analysis: Fundamentals and practices. *Ocean. Model.* **2018**, *121*, 49–75. [CrossRef]

18. Lonin, S.A. Lagrangian model for oil spill diffusion at sea. *Spill Sci. Technol. Bull.* **1999**, *5*, 331–336. [CrossRef]

19. Lebreton, L.C.M.; Greer, S.D.; Borrero, J.C. Numerical modelling of floating debris in the world's oceans. *Mar. Pollut. Bull.* **2012**, *64*, 653–661. [CrossRef]

20. Dawson, M.N.; Gupta, A.S.; England, M.H. Coupled biophysical global ocean model and molecular genetic analyses identify multiple introductions of cryptogenic species. *Proc. Natl. Acad. Sci. USA* **2005**, *102*, 11968–11973. [CrossRef]

21. Hertwig, D.; Burgin, L.; Gan, C.; Hort, M.; Jones, A.; Shaw, F.; Witham, C.; Zhang, K. Development and demonstration of a Lagrangian dispersion modeling system for real-time prediction of smoke haze pollution from biomass burning in Southeast Asia. *J. Geophys. Res. Atmos.* **2015**, *120*, 12605–12630. [CrossRef]

22. Williams, R.G.; Follows, M.J. *Ocean Dynamics and the Carbon Cycle: Principles and Mechanisms*; Cambridge University Press: Cambridge, UK, 2011. [CrossRef]

23. PyGNOME. Available online: https://gnome.orr.noaa.gov/doc/pygnome/index.html (accessed on 27 March 2024).

24. Pisso, I.; Sollum, E.; Grythe, H.; Kristiansen, N.; Cassiani, M.; Eckhardt, S.; Arnold, D.; Morton, D.; Thompson, R.; Groot Zwaaftink, C.; et al. The Lagrangian particle dispersion model FLEXPART version 10.4. *Geosci. Model Dev.* **2019**, *12*, 4955–4997. [CrossRef]

25. Adhikari, R.; Agrawal, R.K. An Introductory Study on Time Series Modeling and Forecasting. *arXiv* **2013**, arXiv:1302.6613.

26. Raicharoen, T.; Lursinsap, C.; Sanguanbhokai, P. Application of Critical Support Vector Machine to Time Series Prediction. In Proceedings of the 2003 International Symposium on Circuits and Systems, ISCAS '03, Bangkok, Thailand, 25–28 May 2003; Volume 5, p. V. [CrossRef]

27. Raksha, S.; Graceline, J.S.; Anbarasi, J.; Prasanna, M.; Kamaleshkumar, S. Weather Forecasting Framework for Time Series Data using Intelligent Learning Models. In Proceedings of the 2021 5th International Conference on Electrical, Electronics, Communication, Computer Technologies and Optimization Techniques (ICEECCOT), Mysuru, India, 10–11 December 2021; pp. 783–787. [CrossRef]

28. Chatterjee, A.; Bhowmick, H.; Sen, J. Stock Price Prediction Using Time Series, Econometric, Machine Learning, and Deep Learning Models. In Proceedings of the 2021 IEEE Mysore Sub Section International Conference (MysuruCon), Hassan, India, 24–25 October 2021; pp. 289–296. [CrossRef]

29. Wang, P.; Gurmani, S.H.; Tao, Z.; Liu, J.; Chen, H. Interval time series forecasting: A systematic literature review. *J. Forecast.* **2024**, *43*, 249–285. [CrossRef]

30. Jadon, S.; Milczek, J.; Patankar, A. Challenges and approaches to time-series forecasting in data center telemetry: A Survey. *arXiv* **2021**, arXiv:2101.04224. [CrossRef]

31. Alsharef, A.; Sonia; Kumar, K.; Iwendi, C. Time Series Data Modeling Using Advanced Machine Learning and AutoML. *Sustainability* **2022**, *14*, 15292. [CrossRef]

32. Hamayel, M.J.; Owda, A.Y. A Novel Cryptocurrency Price Prediction Model Using GRU, LSTM and bi-LSTM Machine Learning Algorithms. *AI* **2021**, *2*, 496. [CrossRef]

33. Yamak, P.T.; Yujian, L.; Gadosey, P.K. A Comparison between ARIMA, LSTM, and GRU for Time Series Forecasting. In Proceedings of the 2019 2nd International Conference on Algorithms, Computing and Artificial Intelligence, Sanya, China, 20–22 December 2019; pp. 49–55. [CrossRef]

34. Eriksen, M.; Lebreton, L.C.M.; Carson, H.S.; Thiel, M.; Moore, C.J.; Borerro, J.C.; Galgani, F.; Ryan, P.G.; Reisser, J. Plastic Pollution in the World's Oceans: More than 5 Trillion Plastic Pieces Weighing over 250,000 Tons Afloat at Sea. *PLoS ONE* **2014**, *9*, e111913. [CrossRef] [PubMed]

35. Ali, A.M.; Zhuang, H.; VanZwieten, J.; Ibrahim, A.K.; Chérubin, L. A Deep Learning Model for Forecasting Velocity Structures of the Loop Current System in the Gulf of Mexico. *Forecasting* **2021**, *3*, 953. [CrossRef]

36. Choi, H.M.; Kim, M.K.; Yang, H. Deep-learning model for sea surface temperature prediction near the Korean Peninsula. *Deep Sea Res. Part II Top. Stud. Oceanogr.* **2023**, *208*, 105262. [CrossRef]

37. Tensorflow TensorFlow TimeseriesGenerator—TensorFlow Core v2.13.0. Available online: https://www.tensorflow.org/api_docs/python/tf/keras/preprocessing/sequence/TimeseriesGenerator (accessed on 29 August 2024).

38. Abadi, M.; Agarwal, A.; Barham, P.; Brevdo, E.; Chen, Z.; Citro, C.; Corrado, G.; Davis, A.; Dean, J.; Devin, M.; et al. TensorFlow: Large-Scale Machine Learning on Heterogeneous Systems. 2015. Available online: https://www.tensorflow.org/ (accessed on 29 August 2024).

39. Aijaz, S.; Colberg, F.; Brassington, G.B. Lagrangian and Eulerian modelling of river plumes in the Great Barrier Reef system, Australia. *Ocean. Model.* **2024**, *188*, 102310. [CrossRef]

40. Yadav, H.; Thakkar, A. NOA-LSTM: An efficient LSTM cell architecture for time series forecasting. *Expert Syst. Appl.* **2024**, *238*, 122333. [CrossRef]

41. Naderalvojoud, B.; Hernandez-Boussard, T. Improving machine learning with ensemble learning on observational healthcare data. *AMIA Annu. Symp. Proc.* **2024**, *2023*, 521–529.

42. Vaswani, A.; Shazeer, N.; Parmar, N.; Uszkoreit, J.; Jones, L.; Gomez, A.N.; Kaiser, L.u.; Polosukhin, I. Attention is All you Need. In *Proceedings of the Advances in Neural Information Processing Systems*; Guyon, I., Luxburg, U.V., Bengio, S., Wallach, H., Fergus, R., Vishwanathan, S., Garnett, R., Eds.; Curran Associates, Inc.: Red Hook, NY, USA, 2017; Volume 30.